Parolai, S., Ansal, A., Kurtulus, A., Strollo, A., Wang, R., Zschau, J. (2009): The Ataköy vertical array (Turkey): insights into seismic wave propagatin in the shallow-most crustal layers by waveform deconvolution. - Geophysical Journal International, 178, 3, pp. 1649—1662.

DOI: http://doi.org/10.1111/j.1365-246X.2009.04257.x

Geophys. J. Int. (2009) **178,** 1649–1662 doi: 10.1111/j.1365-246X.2009.04257.x

The Ataköy vertical array (Turkey): insights into seismic wave propagation in the shallow-most crustal layers by waveform deconvolution

Stefano Parolai,[1] Atilla Ansal,[3] Asli Kurtulus,[3] Angelo Strollo,[1,2] Rongjiang Wang[1] and J. Zschau[1]

[1] *Deutsches GeoForschungs Zentrum - GFZ - Section* 2.1 *"Earthquake Risk and Early Warning", Telegrafenberg,* D-14473 *Potsdam, Germany. E-mail: parolai@gfz-potsdam.de*

[2] *Institute of Geosciences, Universität Potsdam, Karl-Liebknecht Strasse,* 14476 *Potsdam, Germany*

[3] *Boğaziçi Üniversitesi, Kandilli Rasathanesi ve Deprem Araştırma Enstitüsü, Department of Earthquake Engineering,* 34684 *Çengelköy, Istanbul, Turkey*

Accepted 2009 May 15. Received 2009 May 15; in original form 2008 December 12

SUMMARY

A vertical array of accelerometers was installed in Ataköy (western Istanbul) with the long-term aim of improving our understanding of *in situ* soil behaviour, to assess the modelling and parametric uncertainties associated with the employed methodologies for strong-motion site-response analysis, and for shallow geological investigations. Geotechnical and geophysical investigations were carried out to define the subsoil structure at the selected site. Data associated with 10 earthquakes ($2.7 < M < 4.3$) collected during the first months of operation of the array were used to image the upgoing and downgoing waves by deconvolution of waveforms recorded at different depths. Results have shown that the velocity of propagation of the imaged upgoing and downgoing waves in the borehole is consistent with that of *S* or *P* waves, depending on the component of ground acceleration analysed but independent of the chosen signal window. In particular, an excellent agreement was found between the observed upgoing and downgoing wave traveltimes and the ones calculated using a model derived by seismic noise analysis of array data. The presence of a smaller pulse on the waveforms obtained by deconvolution of the horizontal components suggests both internal *S*-wave reflection and *S*-to-*P* mode conversion, as well as a not normal incidence of the wavefield. The presence of a pulse propagating with *S*-wave velocity in the uppermost 25 m in the waveforms obtained by the deconvolution of the vertical components suggests *P*-to-*S* mode conversion. These evidences imply that, even when site amplification is mainly related to 1-D effects, the standard practice in engineering seismology of deconvolving the surface recording down to the bedrock using an approximate *S*-wave transfer function (generally valid for vertical incidence of SH waves) might lead to errors in the estimation of the input ground motion required in engineering calculations. Finally, downgoing waves with significant amplitudes were found down to 70 m and even to 140 m depth. This result provides a warning about the use of shallow borehole recordings as input for the numerical simulation of ground motion and for the derivation of ground motion prediction relationships.

Key words: Interferometry; Earthquake ground motions; Site effects.

INTRODUCTION

It has long been recognized that ground shaking during earthquakes can be significantly modified by the mechanical properties of surficial geological formations, typically referred to as local soil conditions. Therefore, realistic ground-motion predictions of future earthquakes can be only achieved by combining realistic source, wave-propagation and site-response models. The increasing number of observations over the last few decades has contributed greatly towards the understanding of strong motion site effects by the engineering and seismological communities, leading to advancements in the state of knowledge and modelling of *in situ* sediment response (Field *et al*. 1997). Nonetheless, finer resolution and more effective representation of the involved physics in the near surface require a good estimate of the input motion and of wave propagation in shallow layers. For this, by far, the best source of information is provided by downhole arrays.

Downhole measurements are a valuable complement to *in situ* and laboratory geotechnical investigation techniques. In fact, they provide critical constraints for both the interpretation methods for

surface observations as well as information on the real material behaviour and overall site response over a wide range of loading conditions (Assimaki *et al*. 2008). The amount and quality of information from downhole arrays in seismically active areas is the key to both improving our understanding of *in situ* soil behaviour, to assess the modelling and parametric uncertainties associated with employed methodologies for strong-motion site-response analysis, and for shallow geological investigations.

With this aim, a vertical array of accelerometers was installed in Ataköy (western Istanbul) where, during the 1999 Kocaeli earthquake (Tibi *et al*. 2001) the peak ground acceleration was measured to be 0.17 g, much higher than the values recorded (0.05–0.09 g) east of the Golden Horn by the Kandilli Observatory and Earthquake Research Institute (KOERI) rapid response system (Dalgic 2004). It is worth noting that east of the Golden Horn the Palaeozoic rocks of the Trakya formation are outcropping while in Ataköy, Oligocene and Miocene sediments overlie the Palaeozoic bedrock, suggesting the influence of site effects on ground motion. In this study, we analysed the recordings of 10 earthquakes by means of a deconvolution approach. Although the use of the Fourier spectra amplitude ratio (uphole to downhole or with a reference station) is well known in engineering seismology (e.g. Safak 1997), the deconvolution of seismograms (therefore also retaining information about phase, and its interpretation in the time domain) has found few applications (Trampert *et al*. 1993; van Vossen *et al*. 2004; van Vossen *et al*. 2005). However, recently, Mehta *et al*. (2007a,b), starting from the similarity between deconvolution and the cross-correlation tool used in seismic interferometry (amongst many others Lobkins & Weaver 2001; Schuster *et al*. 2004; Shapiro & Campillo 2004; Snieder *et al*. 2006; Halliday & Curtis 2008), showed that the deconvolution of waveforms recorded by a vertical array can provide useful insight into the wavefield propagation in the uppermost crustal layers.

Following a similar approach, but making use of a larger available data set, in this study we first describe the array and the available geotechnical and geophysical data. Second, we test two different deconvolution procedures. Third, we show and discuss the results obtained by deconvolving only the part of the seismograms dominated by different seismic phases. Finally, we report and discuss, taking advantage of the available *in situ* analysis data, the results obtained by deconvolving the seismograms using either the surface or the deepest accelerometric station as a reference.

ARRAY DESCRIPTION

In 2005 December, a drilling program consisting of four boreholes of 25, 50, 70 and 140 m deep was realized (ZETAŞ® 2006) in western Istanbul (Turkey) in the district of Ataköy (Fig. 1). PVC pipes were installed in the borehole and the space between the PVC pipes and boreholes was filled with cement grout. Within the 140 m deep borehole, based on the encountered subsoil conditions,

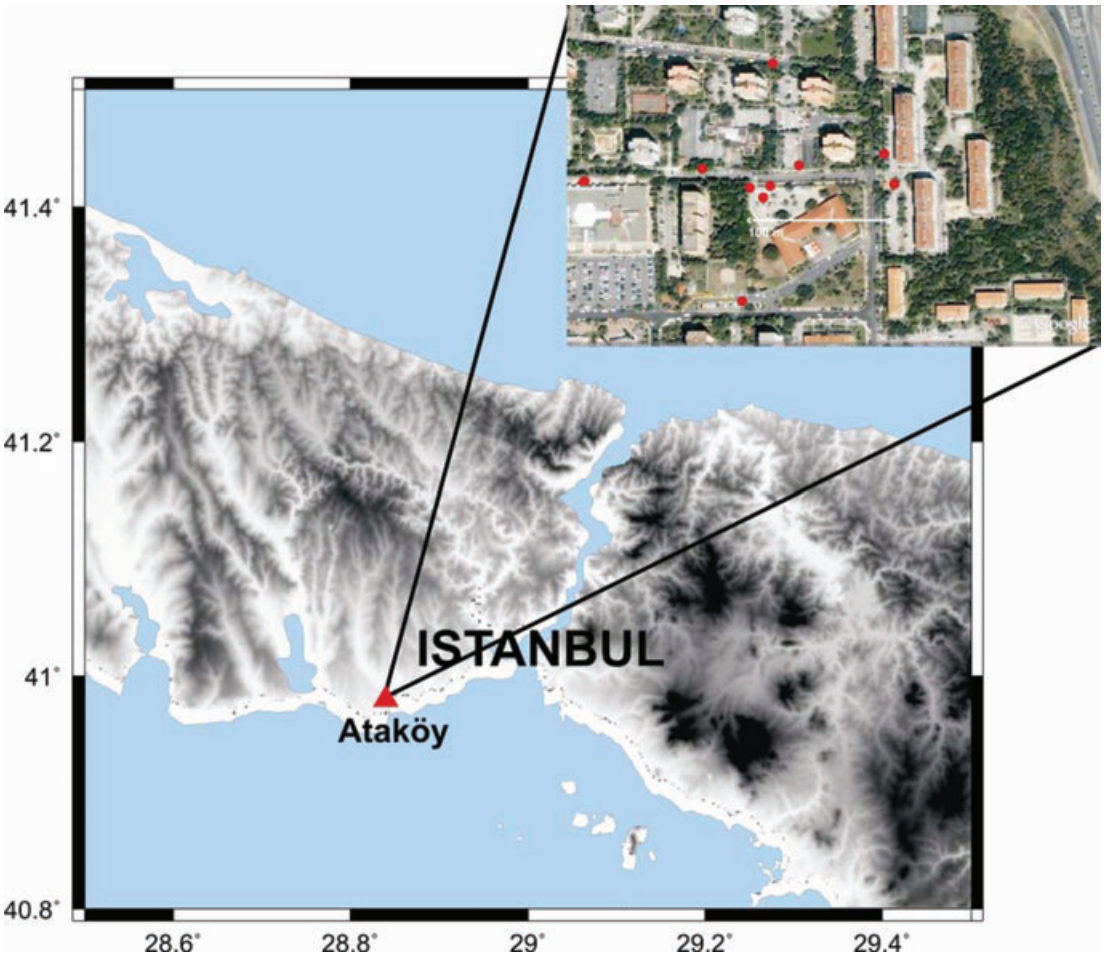

Figure 1. Map of the area under investigation. The triangle shows the location of the vertical array and of the seismic noise microarray. The seismic noise microarray configuration is shown as an inset.

representative and/or undisturbed soil samples were obtained and Standard Penetration Test (SPT) carried out at regular intervals of 1.5 m. The water table was encountered at 15 m depth.

The array was instrumented with three Shallow Boreholes accelerometers (SBEPI) at 25, 50 and 70 m depth and a Down borehole accelerometer (ES-DH) at 140 m depth, connected to a 12 channel K2 at the surface. Additionally, a K2 with internal episensor was installed at the surface. Data can be accessed via Internet by the KOERI and the Helmholtz Centre Potsdam GFZ German Research Centre for Geosciences (GFZ).

A total of 60 SPT samples and three undisturbed samples (from depths 35, 49 and 52 m) were chosen for laboratory tests, including sieve analysis, with the aim of estimating natural moisture content and Atterberg's limits.

Fig. 2 summarizes the stratigraphy at the site and the results of the SPT tests. Note that refusal was defined when the blowcount was greater than 100 blows per 50 mm. Within the first 15 m depth, the subsoil is composed of light brown, hard gravelly sandy clay. Below this layer, limestone with a low Rock Quality Designation (RQD) and clay interlayers were found down to 35 m depth. Below this depth until the bottom of the deepest borehole, hard/very dense sandy clay/clayey sand layers were encountered.

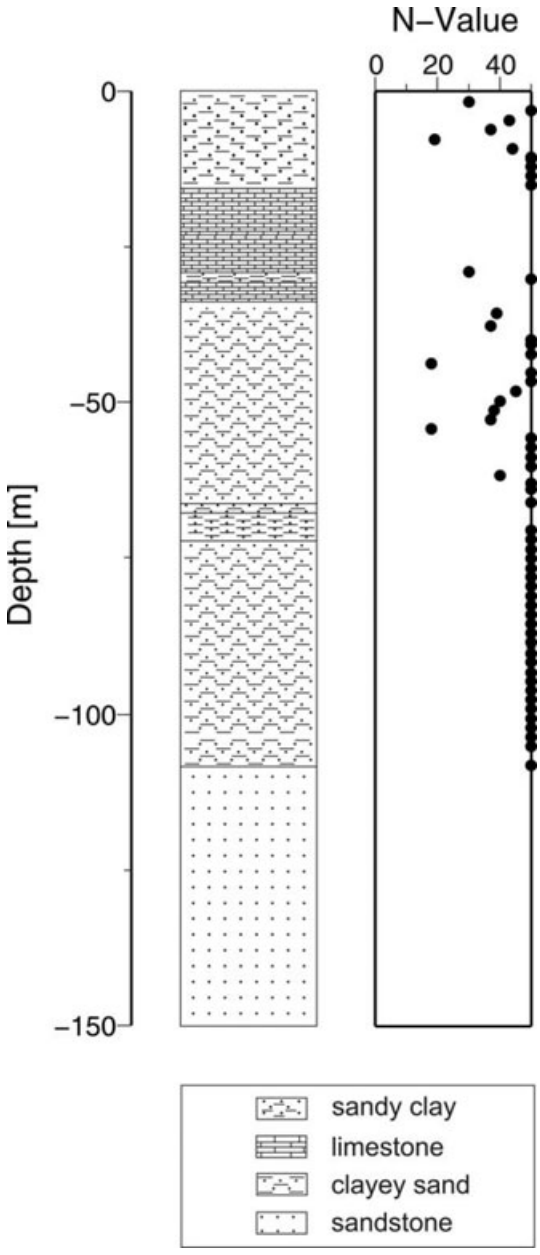

Figure 2. Left-hand panel: Ataköy vertical array stratigraphic column. Right-hand panel: SPT values versus depth.

SUSPENSION *PS* VELOCITY LOGGINGS

Suspension *PS* velocity logging is a method for determining shear and compressional wave velocity (*Vs* and *Vp*) profiles of soils and rocks. Measurements are made in a single, cased/uncased, fluid filled borehole (Nigor & Imai 1994). The measurement procedure is as follows. A probe, that has a solenoid source at its lower end and two geophones mounted at a distance of 1 m, is lowered to the bottom of the borehole and then raised at specific depth intervals to take measurements. At each depth the source is activated in one horizontal direction and the output, which would include *S* waves, is measured by the two horizontal geophones. The source is then activated in the reverse direction, producing a reverse polarity wave. Finally, the source is activated in the first direction again and the signal in the vertical component (mainly dominated by *P* waves) is recorded. The probe is then raised to the next depth of interest. Typically, measurements are carried out at 0.5–1 m intervals. The analysis consists of picking the first break or the first peak for estimating the arrival time and then, knowing the distance between the geophones, calculating the velocity over the corresponding depth interval.

In Ataköy a *PS* Logging system manufactured by OYO Corporation, Japan, was used. It consists of a probe (Model 3302A), cable, winch (Type 350) and logger (control/recording, Model 3660A). The probe is approximately 8 m in length. The source used produces energy mainly in the frequency band 500–5000 Hz. The test was carried out in 2006 November.

The results of the *PS* logging test are shown in Fig. 3. The results show that there is a general trend of increasing *Vs* with depth. The average *S*-wave velocity in the uppermost 35 m is about 220 m s^{-1}, after which it increases to an average of about 530 ms^{-1} over the depth interval 35–100 m depth, consistent with the observed stratigraphical variation (Fig. 2). Below a depth of 100 m, the velocity values are more scattered and span between 600 and 1000 m s^{-1}.

MICROARRAY MEASUREMENTS

The recent improvements in the quality of seismic instrumentation and in computing power have enabled seismologists to redirect their attention towards analysing seismic noise recorded by arrays (e.g. Horike 1985; Hough *et al*. 1992; Ohori *et al*. 2002; Okada 2003; Scherbaum *et al*. 2003; Parolai *et al*. 2005), a method originally proposed by Aki (1957). The objective of such studies is the determination of (local) shear wave velocity profiles down to depths prohibitive both in terms of the costs they would require and the technical demands necessary for standard geophysical methods in urban areas.

Therefore, in order to estimate the *S*-wave velocity structure at the vertical array site (Ataköy), an array of 12 stations was installed in the vicinity of the vertical array installation on 2005 September 20 to measure seismic noise (Fig. 1). The stations operated simultaneously for more than 1 hr, recording noise at 100 samples s^{-1}, which is adequate for the interstation distance considered

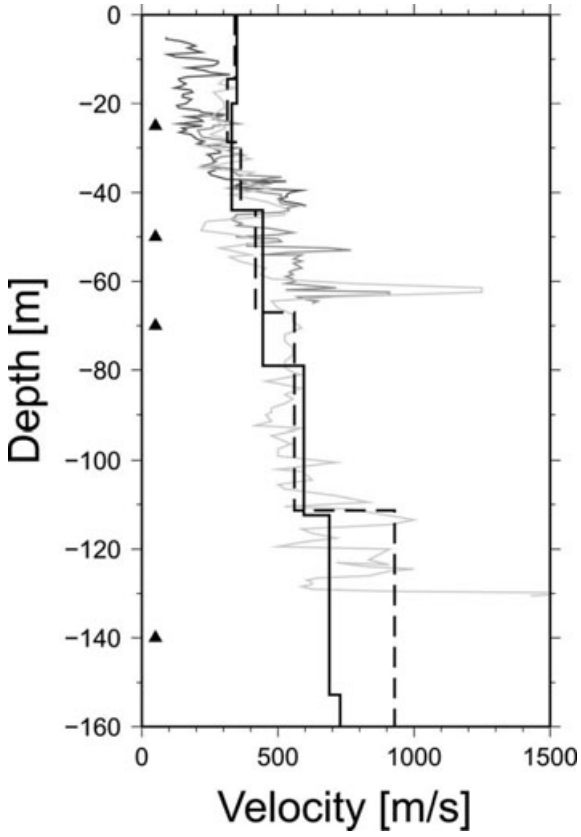

Figure 3. *S*-wave velocities for Ataköy inferred from the *PS* logging carried out in the 50 (dark grey), 70 (grey) and 140 m (light grey) deep boreholes and from the joint inversion performed by inverting only the *S*-wave velocity and the thickness of the layers (black line) and following the Picozzi and Albarello (2007) inversion scheme (dashed line). Triangles indicate the installation depth of the accelerometers.

(∼10 to ∼230 m). Every station was equipped with a 24-bit digitizer connected to a Mark L-4C-3-D 1 Hz sensor and GPS timing. For the analysis, the data recorded by each station of the array were divided into 60 s windows. A total of 44 non-overlapping windows were considered. Only the vertical component was analysed to obtain the Rayleigh wave dispersion curve. Recordings were corrected for the instrumental response considering the calibration parameters of each sensor. Due to malfunctions, data from two stations could not be used. Fig. 1 shows the array geometry.

The calculation of the dispersion curve (Fig. 4) was carried out following Ohori *et al*. (2002); Okada (2003) and Parolai *et al*. (2006) by applying the Extended Spatial Correlation (ESAC) method.

Horizontal-to-vertical (H/V) spectral ratios (Nakamura, 1989) from the 44 windows of noise recordings at each station were also calculated. Their Fourier spectra were computed and smoothed using a Konno & Ohmachi (1998) window with the coefficient b fixed to 40. For every station a mean H/V curve was calculated using a logarithmic average of the individual H/V curves. Fig. 4, bottom right-hand panel, shows the mean H/V curve at the central station of the array used in the inversion (grey filled circle), and the H/V curves for each station (grey lines).

The inversion was performed following Parolai *et al*. (2005) and used the modified Genetic Algorithm (GA) proposed by Yamanaka & Ishida (1996). The *P*-wave velocity was fixed to 700 m s^{-1} in the first layer, and then chosen to increased from 1400 m s^{-1} in the second layer to 1800 m s^{-1} in seventh one. The half-space *P*-wave velocity was fixed to 2250 m s^{-1}. The number of layers was chosen after trial and error tests in order to avoid overparametrization and to ensure proper representation of the velocity with depth (Parolai *et al*. 2006). The results show a satisfactory agreement between the observed and calculated dispersion and H/V curves (Fig. 4).

Furthermore, the inversion was also performed by Picozzi *et al*. (2009) following the scheme proposed by Picozzi & Albarello (2007), attempting also to invert for the Poisson's ratio. The two inversions produced very similar *S*-wave velocity profiles (Fig. 3), while the *P*-wave structure was somewhat different. This highlights the weak dependency of the phase velocity and H/V curve inversion on the *Vp* structure.

In both cases, the dispersion curve constrains the model only down to 130–180 m. The deeper part is constrained by the H/V data alone. All models lying inside the minimum cost +10 per cent show little variability down to 230 m depth. Below 230 m, the larger variability indicates that the trade-off between velocity and thickness of the layers is not fully solved by the H/V inversion.

These results are also shown in Fig. 3, where an excellent agreement is noted in terms of the average velocities, considering in particular the different wavelengths of the signal used in the *PS* logging and in the microarray, as well as the different volume examined around the vertical array (tens of centimetres and hundred of metres for *PS* logging and the microarray, respectively) that determine the velocity profile.

DECONVOLUTION OF THE WAVEFIELD

Since 2006 December, ten seismic events (Table 1) with magnitudes between 2.7 and 4.6 have been recorded by the Ataköy vertical array (Fig. 5). Since the orientation of the sensor at 25, 50 and 70 m depth is unknown, before performing an analysis including the horizontal components a correction should be performed. However, the algorithms generally used for estimating the orientation errors of downhole accelerometers (e.g. Chiu *et al*. 1994; Chiu & Huang 2003; Huang *et al*. 2005) take advantage of the high-energy low-frequency content of strong earthquakes. Since our data set is mainly composed of small magnitude events rich in high frequencies, these techniques cannot be applied since the scattering associated with such a frequency range strongly affects wave propagation from the bottom of the array to the surface. Thus, at the moment we decided to use an alternate approach to obtain a 'horizontal' component at each level for the events used in the following analysis. The approach, similar to Seale & Archuleta (1989), is simply based on rotating the recorded horizontal components to the direction that determines the maximum spectral energy. The recordings rotated in this direction were then used for the subsequent analysis.

The application of the standard spectral ratio between the Fourier transform of the corrected signals recorded at the surface and within the boreholes with that recorded at the array bottom accelerometer (140 m) showed a peak at nearly 1 Hz (Fig. 6). The independence of frequency of this peak on the station depth suggests that it might be due to a spectral trough at that frequency in the Fourier transform of the bottom station recording due to destructive interference of upgoing and downgoing waves. In fact, the period of nearly 1 second corresponds to four times the traveltime of *S* waves as estimated by the microarray and the *PS*-logging measurements. In order to assess if the downhole recordings are affected by downgoing waves, we deconvolved the wavefield recorded in the boreholes with that recorded at the surface, similarly to Mehta *et al*. (2007a,b).

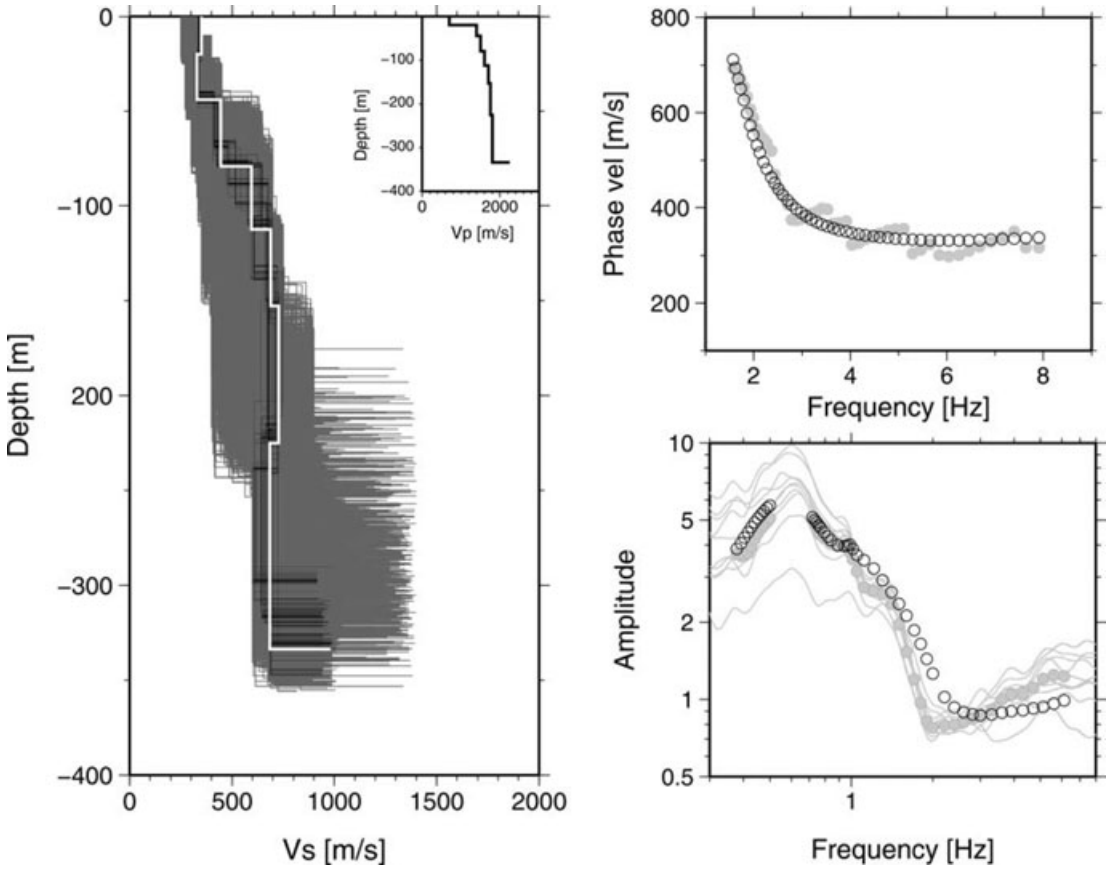

Figure 4. Left-hand panel: joint inversion results for Ataköy using the Parolai *et al*. (2005) inversion scheme: all tested models (dark grey), the minimum misfit model (white), models lying inside the minimum misfit +10 per cent range (black). The inset shows the *P*-wave velocity model used in the joint inversion procedure. Bottom right-hand panel: the observed H/V spectral ratio used in the inversion (grey circles) and calculated (white circles) one. Grey lines show the H/V spectral ratio for all stations of the array. Top right-hand panel: the observed (grey circles) and calculated (white circles) apparent phase velocities.

Table 1. List of events used in this study.

Event ID	Origin time (dd/mm/yyyy/hh:mm:s)	Latitude (°)	Longitude (°)	Depth (km)	*M*
1	19/12/2006/19:15:36.9	40.39	28.31	11.6	4.3
2	14/11/2007/09:02:13	40.84	28.86	15	2.8
3	17/01/2008/04:23:53	40.74	29.048	5.3	3.0
4	03/02/2008/14:57:08	40.764	29.198	5.3	3.0
5	12/03/2008/18:53:38.5	40.84	28.99	10	4.6
6	01/06/2008/03:35:30.6	40.07	26.77	20	4.4
7	06/06/2008/22:57:18	41.11	28.84	6	3.4
8	05/10/2008/09:04:05	40.65	29.017	8.5	4.1
9	25/10/2007/11:02:32.4	40.85	28.69	5	2.7
10	08/02/2007/13:18:17.4	40.84	28.71	11	2.8

Choosing the deconvolution approach

The deconvolution of ground motion recorded at a depth $z1$ with that at depth $z2$ (where $z = 0$ at the surface) can be written in the frequency domain as

$$S(\omega) = \frac{u(z1, \omega)}{u(z2, \omega)}, \tag{1}$$

where $u(z1, \omega)$ and $u(z2, \omega)$ are the Fourier transform of the motion recorded at depths $z1$ and $z2$, respectively. However, the deconvolution operation is applied to data corrupted by noise and therefore, since this problem is ill-conditioned, small errors in the data could lead to solutions unacceptable from a physical point of view. In particular, the condition number α, defined as

$$\alpha = \frac{u(z2, \omega)\,\max}{u(z2, \omega)\,\min}, \tag{2}$$

acts as an amplification factor that controls the error transfer from the recorded data to site response (Bertero & Boccacci 1998). In eq. (2), $u(z2, \omega)$max and $u(z2, \omega)$min are the maximum and the minimum values of the Fourier amplitude spectra $|u(z2, \omega)|$. A large condition number implies numerical instability.

To avoid this instability, a regularized Tikhonov deconvolution can be used (Tikhonov & Arsenin 1977; Bertero & Boccacci 1998;

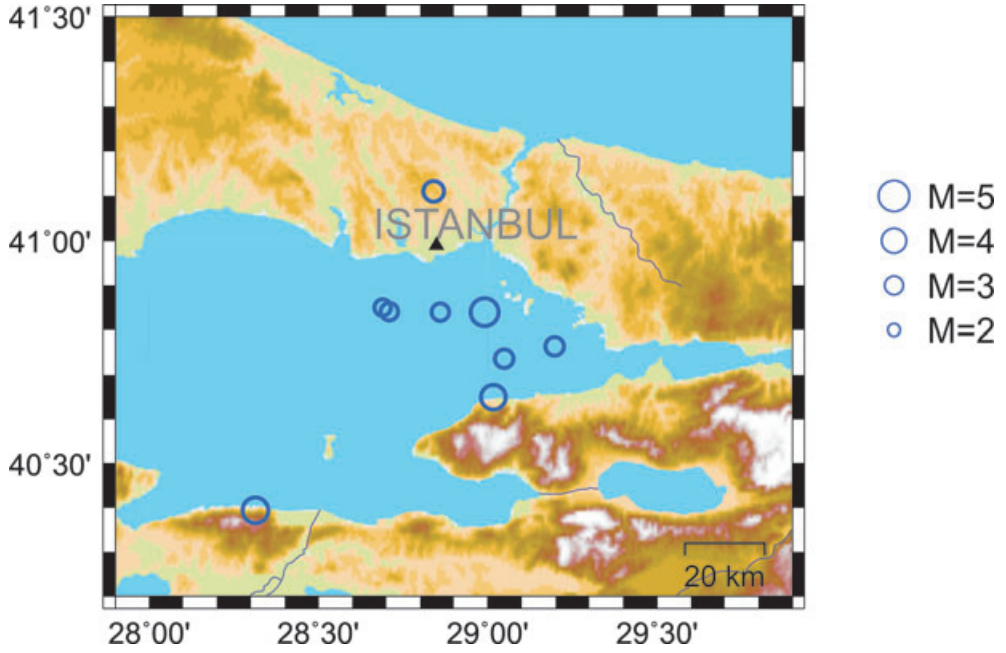

Figure 5. Location of the Ataköy vertical array (triangle) and the epicentres (circles) of the earthquakes used in this study. Note that the epicentre of one of the earthquakes reported in Table 1 (ID6) lies outside of the depicted area.

Mehta *et al*. 2006a,b):

$$S_\varepsilon(\omega) = W_\varepsilon(\omega)\frac{u(z1,\omega)}{u(z2,\omega)}, \tag{3}$$

where $S(\omega)$ denotes the Fourier spectrum of the deconvolved wavefield and

$$W_\varepsilon(\omega) = \frac{|u(z2,\omega)|^2}{|u(z2,\omega)|^2 + \varepsilon} \tag{4}$$

is the filter. ε refers to a constant added to the denominator to prevent the numerical instability of eq. (1)

Nonetheless, other regularization techniques can be adopted. In this study, we tested also a different Tikhonov regularization technique, known as the Landweber algorithm, described in detail in Bertero & Boccacci (1998), that also allows us to easily include constraints in the deconvolution (Bertero *et al*. 1997). This algorithm is based on an iterative scheme described as follows:

$$S_n(\omega) = W_n(\omega)\frac{u(z1,\omega)}{u(z2,\omega)}, \tag{5}$$

where

$$W_n(\omega) = 1 - (1 - \tau|u(z2,\omega)|^2)^n \tag{6}$$

is the Landweber filter and $S_n(\omega)$ denotes the Fourier spectrum of the deconvolved wavefield at the nth iteration. The behaviour of the filter $Wn(\omega)$ depends on both the number of iterations n and on the relaxation parameter τ. The latter determines the rate of convergence of the iterative scheme and must satisfy the following condition:

$$0 < \tau < \frac{2}{u(z2,\omega)\max^2}. \tag{7}$$

In particular, $\tau < \frac{1}{u(z2,\omega)\max^2}$ increases tolerance to noise, but slows down the rate of convergence (Bertero & Boccacci 1998). For a fixed value of the relaxation parameter τ, the choice of the number of iterations settles the filtering level: low values of n lead to highly filtered solutions while if $n \to \infty$ the iterative method converges to the generalized solution (i.e. the minimum norm least-square solution) (Bertero & Boccacci 1998).

Since the choice of the ε and n parameters is crucial for the degree of filtering of the obtained solution, we tested both approaches, to evaluate which one is most suitable for our case. To this regard, we considered as an example the 140 m depth and surface recordings of the earthquake that occurred on 2008 March 12 M 4.6 (ID5 in Table 1). The record at the surface was used as the reference.

In order to apply eq. (3), ε was chosen to vary between 1 and 50 per cent of the average spectral power of $u(0,\omega)$. To apply the algorithm of eq. (5), we set, following Bindi *et al*. (2000),$\tau = \frac{1}{u(0,\omega)\max^2}$ and we allow the n parameter to vary between 10 and 4360.

Fig. 7 (left-hand panel) shows the results obtained using eq. (5) when the n value increases from 10 to more than 4000 (from dark to light grey for increasing values of n), while Fig. 7 (right-hand panel) shows the results calculated when ε decreases from 50 to 1 per cent of the average spectral power of $u(0,\omega)$ (from dark to light grey for decreasing values of ε). For sake of readability, only the results for n equal to 10, 40, 110, 370, 1060, 1540, 1910, 3010 and 4360, and for ε equal to 1, 2, 5, 10, 20 and 50 per cent of the average spectral power of $u(0,\omega)$ are shown. As expected, when increasing the number of iterations in the Landweber algorithm, the solutions obtained are less filtered, but might be more corrupted by noise. Similarly, as expected, decreasing the value of ε leads to less filtered solutions. Taking this into account, solutions obtained with n fixed to 300–500 appear to provide a good compromise between the quality of the retrieved information and the signal-to-noise ratio. A similar result is obtained when the value of ε is set to 10 per cent of the average spectral power of $u(0,\omega)$. Therefore, in this study where other properties of the Landweber algorithm are not exploited, we decided to adopt eq. (3), fixing ε equal to 10 per cent of the average spectral power of $u(0,\omega)$ for the deconvolution of the Ataköy vertical array waveforms.

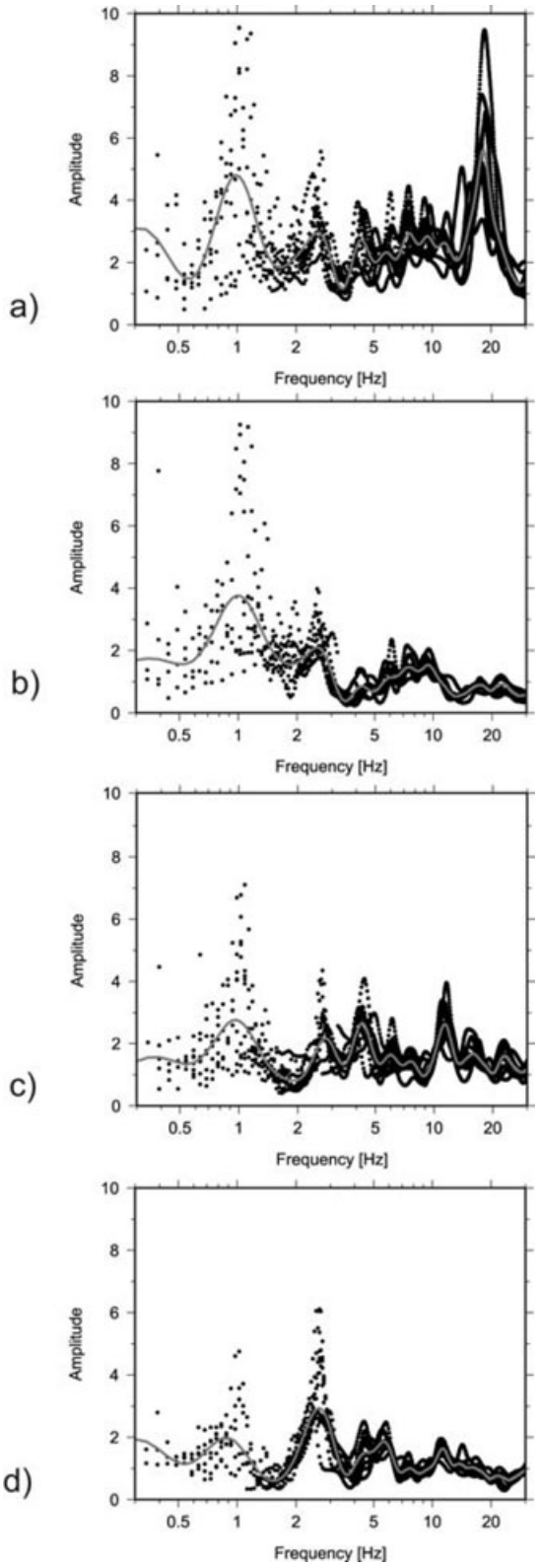

Figure 6. The spectral ratio results, using the station at 140 m depth as the reference, for the station located at the surface (a), at 25 m depth (b), 50 m depth (c) and 70 m depth (d). Black dots indicate spectral ratio values calculated for frequencies with signal-to-noise ratios larger than 3. Due to the limited number of event used, a 1-D trend interpolation (Wessel & Smith 1991) is used to highlight the behaviour of the data.

Selecting the signal window

In order to evaluate the dependence of the deconvolution results on the windows of the signal selected, we extracted windows centred around the main *P* and *S* arrivals. The deconvolution of the waveforms was carried out using both the station at 140 m depth and the one at the surface as a reference. Since results obtained in both cases yield similar conclusions, for the sake of brevity, only results obtained by considering the station at the surface as the reference are shown.

The *M* 4.1 earthquake considered occurred 2008 October 5 at 09:04:05 (Table 1). Figs 8 and 9 show the results obtained by deconvolving the waveforms in the *P*-wave window recorded by the vertical and horizontal components of each of the sensors, respectively.

The figures show that in both cases, the waveforms obtained by deconvolution show up- and downgoing waves. However, the main pulse in the deconvolved waveform is propagating with velocities very close to those estimated by the array measurements for *P* waves, when the vertical component of ground acceleration is considered, and those of *S* waves when the horizontal component is analysed.

Similarly, when the waveforms in the *S*-wave window are deconvolved (Figs 10 and 11), the main upgoing and downgoing pulses are propagating with velocities similar to the estimated *P* wave (when the vertical component is analysed) and *S* wave (when the horizontal component is considered) values.

The independence of the deconvolution results on the signal window used, but their dependence on the component of ground acceleration analysed, confirms the results of Mehta *et al*. (2007a,b). These authors explained this result by *P*-to-*S* mode conversion (that would be able to explain the presence in the *P*-wave window of *S* waves and, similarly, on the *S* wave window of *P* waves) and used a receiver-function-like approach (horizontal-to-vertical spectral ratio) to highlight this effect. Therefore, in the following, the results obtained by waveform deconvolution for all analysed events will be shown for signal windows including the whole recorded time-series.

Finally, it is worth noting that, although the two models derived by array data inversion have quite different *P*-wave velocities (as shown by the traveltime curves in Figs 8–11), the *S* wave ones are in very good agreement. This confirms the weak sensitivity of the dispersion curve of Rayleigh waves on the *P*-wave structure (Xia *et al*. 2003). Importantly, the results obtained by waveform deconvolution show that a *P*-wave velocity model with high velocity already in the second shallow layer (indicating saturation) should be preferred.

In addition, the amplitude of the ground acceleration recorded at 25 m depth is systematically smaller than that recorded at the surface and at 50 m depth. Although *in situ* soil damping measurements are not available, the velocity structure estimated by *PS*-logging and seismic noise data analysis does not suggest the existence of strong attenuation at this level. We therefore, believe that the lower amplitude level recorded might be due to insufficient coupling of the sensor. However, the records at this depth can still be used to assess the existence of upgoing and downgoing waves in the borehole and the good agreement of the main pulse traveltime with the traveltime estimated from the *S*-wave velocity structure confirm this.

Results

Figs 12 and 13 show the deconvolution results for the horizontal component when the station at the surface or the station at 140 m depth is used as the reference, respectively. In general, the upgoing

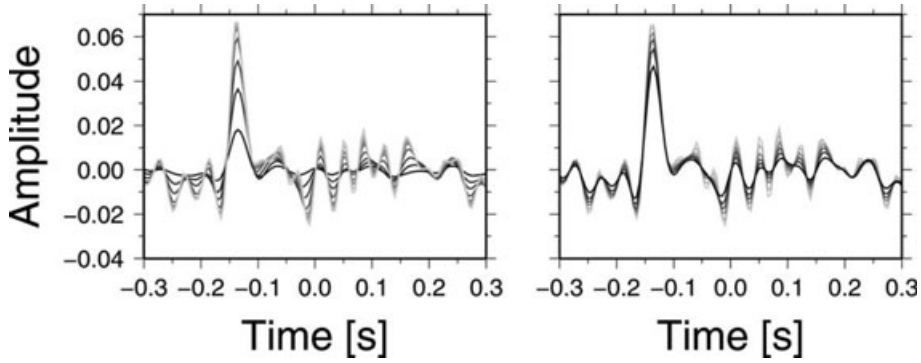

Figure 7. Deconvolved waveforms of the horizontal component recorded at the 140 m depth accelerometer during the 2008 March 12 M 4.6 event (ID5 in Table 1). The station at the surface was used as the reference. Left-hand panel: lines from black to light grey represent solutions obtained for n equal to 10, 40, 110, 370, 1060, 1540, 1910, 3010 and 4360. Right-hand panel: lines from black to light grey represent solutions obtained for ε equal to 50, 20, 10, 5, 2 and 1 per cent of the average spectral power.

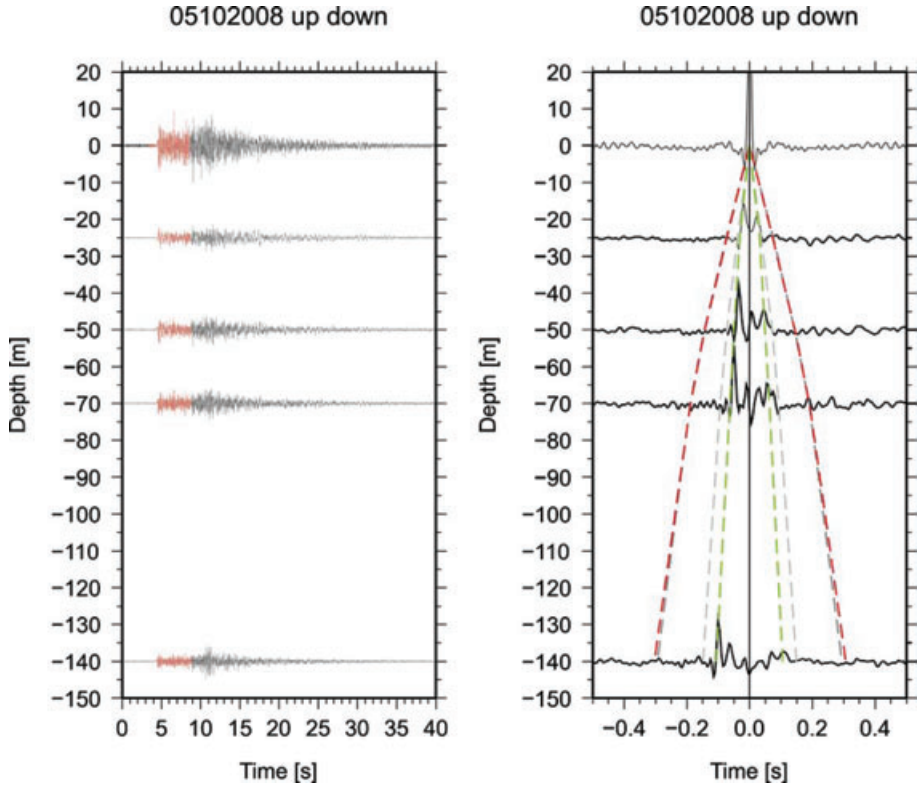

Figure 8. Left-hand panel: vertical component of ground acceleration recorded at different depths. Red lines indicate the window containing P waves. Right-hand panel: the upgoing and downgoing waves. The S-wave traveltimes computed from the velocity model derived using the Parolai *et al*. (2005) inversion scheme (dashed red line) and the S-wave traveltimes computed from the velocity model derived using the Picozzi and Albarello (2007) inversion scheme (dashed dark grey line) are indicated. The P-wave traveltimes computed from the velocity model derived using the Parolai *et al*. (2005) inversion scheme (dashed green line) and the P-wave traveltimes computed from the velocity model derived using the Picozzi and Albarello (2007) inversion scheme (dashed light grey line) are also shown.

and downgoing waves obtained by deconvolving the waveforms of different events are in good agreement, showing that source and path effects (the magnitude and the hypocenter location of the selected earthquakes are different) are removed. Only the results for the surface station in Fig. 13 seem to be corrupted by a higher level of noise.

In Fig. 12, apart from the dominant pulse consistent with the S-wave propagation velocity, between 70 m depth and 25 m depth a smaller pulse is observed. It propagates with a high apparent velocity, close to the expected P wave one, between 25 and 50 m depth and with a velocity closer to the S wave one between 50 and 70 m depth. At 25 m depth, due to the short traveltime, the pulse starts to merge with the main pulse. In Fig. 13, it is seen that one pulse is mainly dominating the waveforms obtained after deconvolution, and it propagates with a velocity consistent with those estimated for the S waves. Smaller pulses arriving after the main ones are only observed between 25 and 50 m.

This result, different from that obtained by Mehta *et al*. (2007a,b), might indicate that due to the short epicentral distance of the analysed data set, the waves arrive at the surface with an incidence far

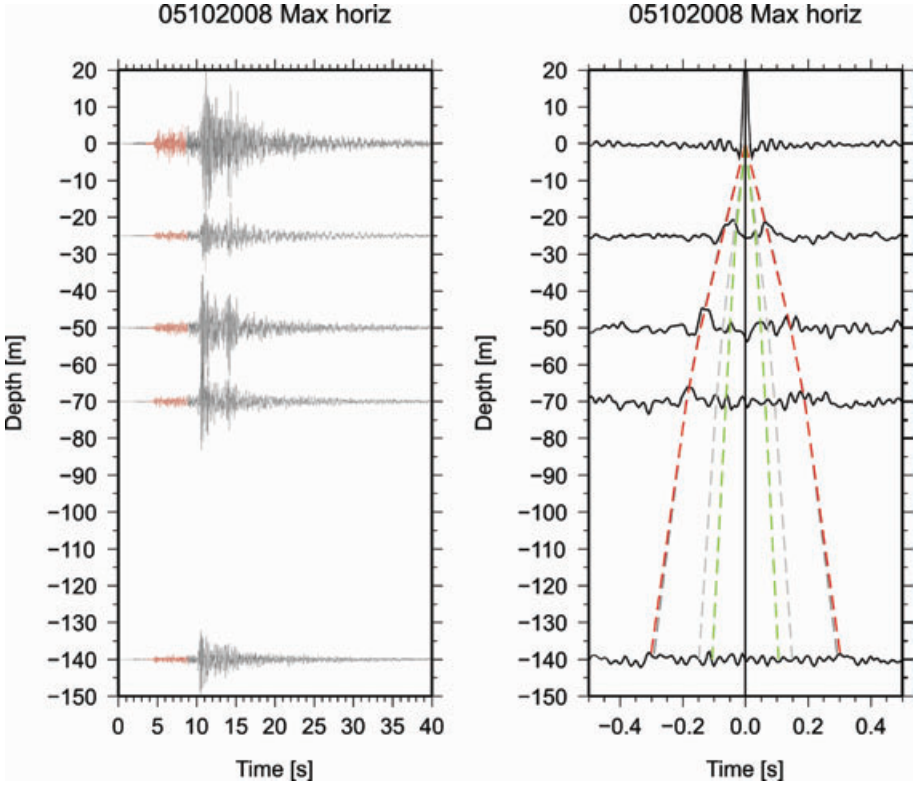

Figure 9. The same as Fig 8, but for the horizontal component.

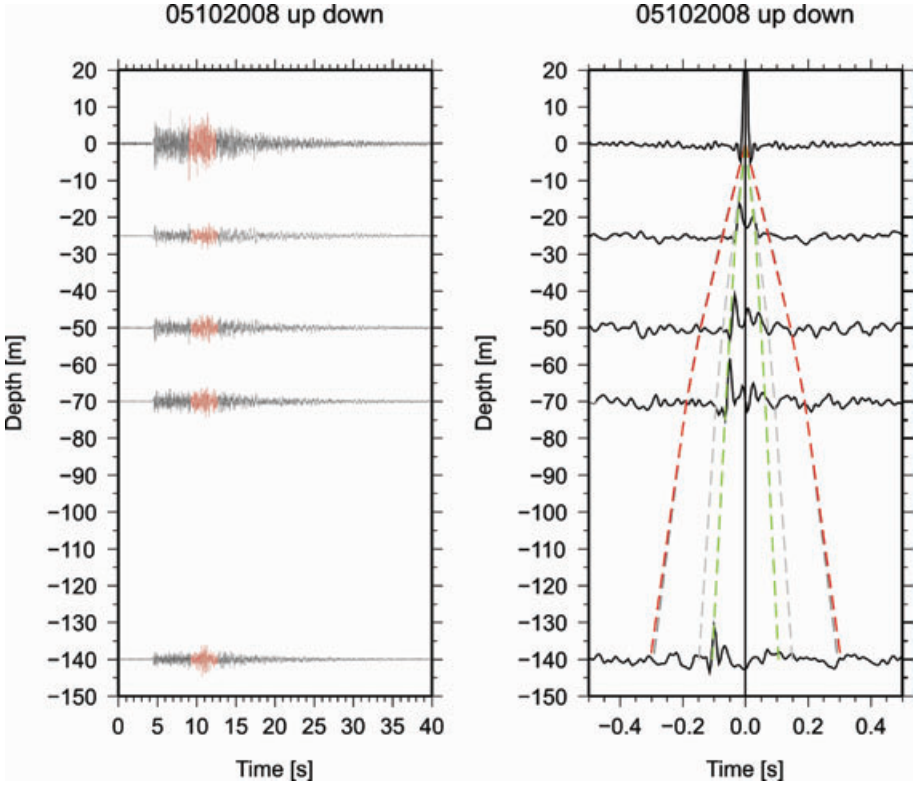

Figure 10. The same as Fig. 8, but with the red lines indicating windows containing *S* waves.

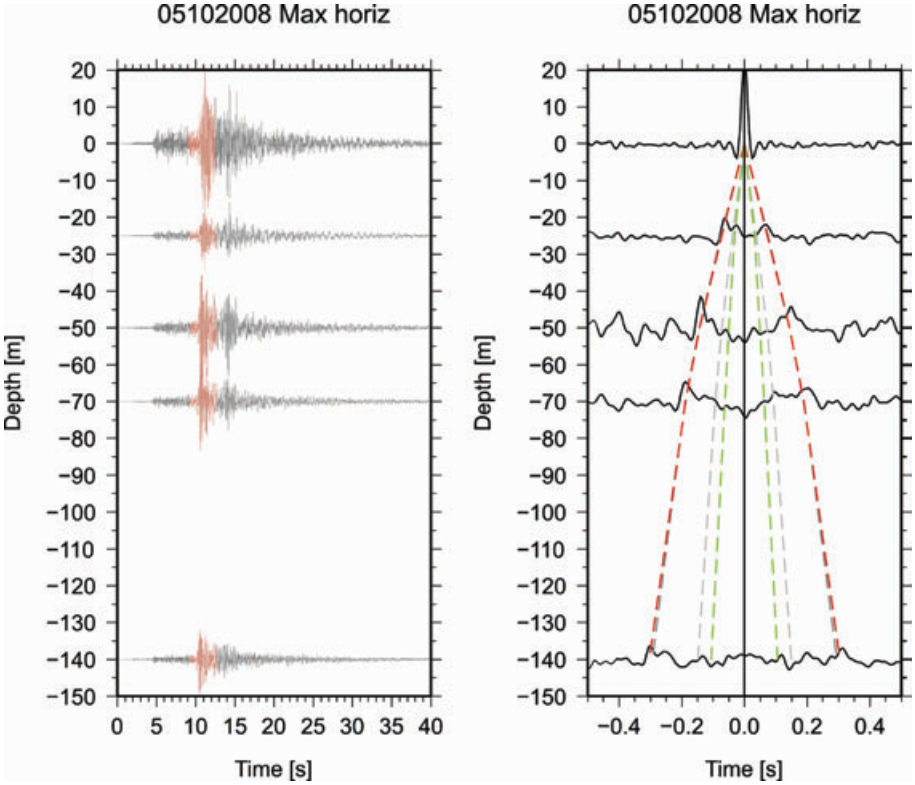

Figure 11. The same as Fig. 9, but with the red lines indicating windows containing *S* waves.

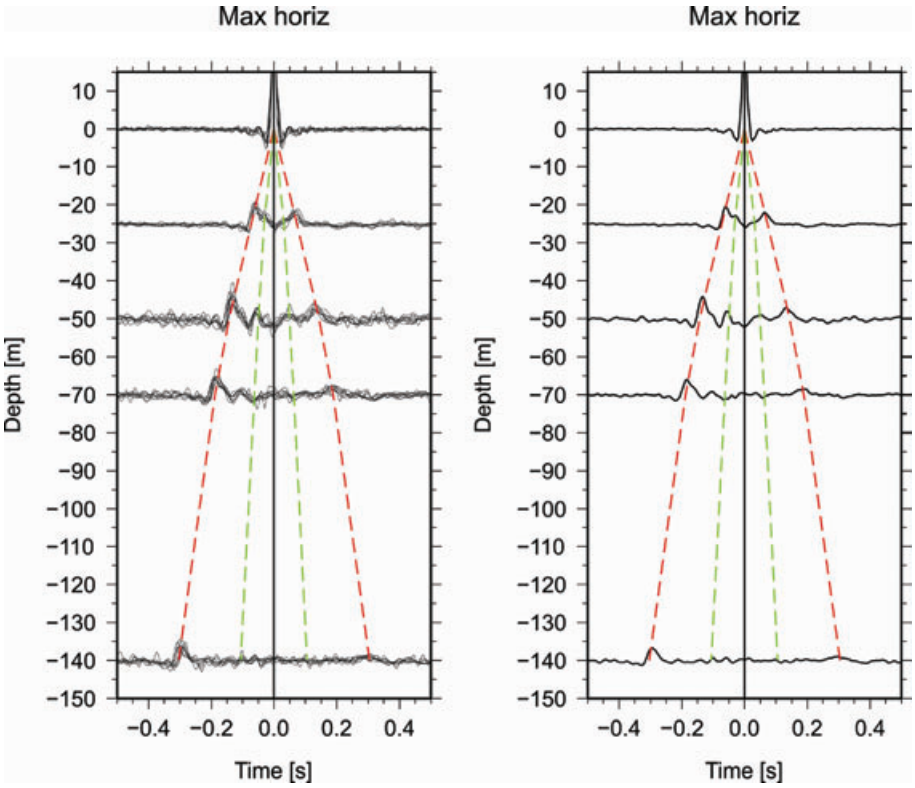

Figure 12. Left-hand panel: the upgoing and downgoing waves obtained by deconvolving the horizontal component waveforms of each of the sensors with the horizontal component waveform recorded by the sensor at the surface. The results for each of the considered earthquakes are shown. Right-hand panel: the stacking of the results depicted in the left-hand panel. The *S*- (dashed red line) and the *P*-waves traveltimes (dashed green line) computed from the velocity model derived using the Parolai *et al*. (2005) inversion scheme are indicated.

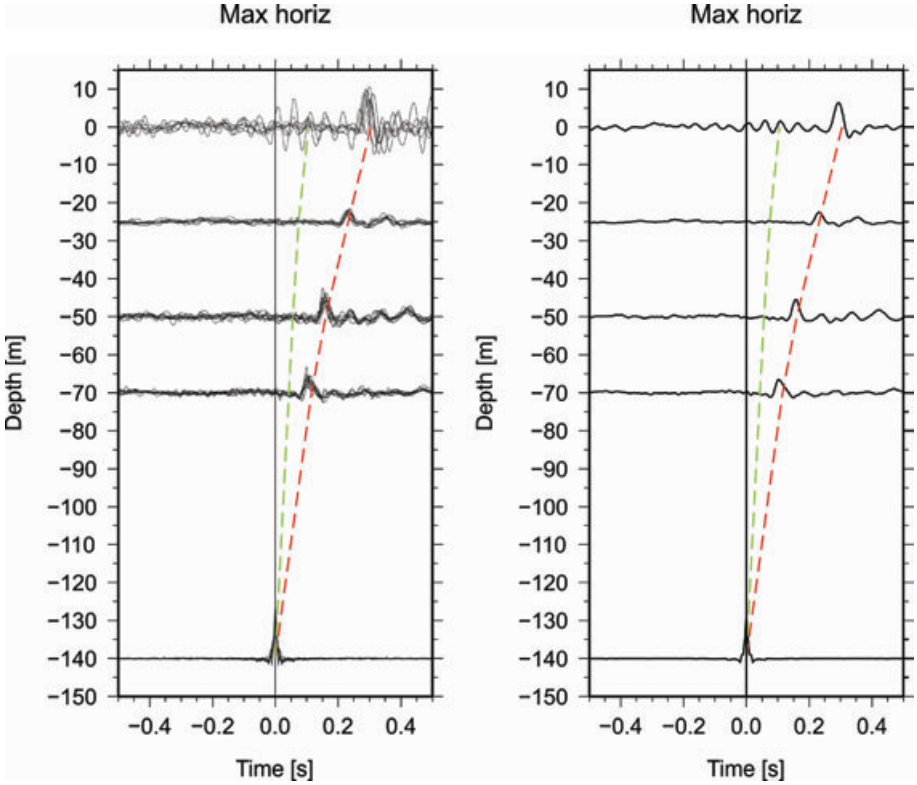

Figure 13. As in Fig. 12, but where the deconvolution was carried out using the station at 140 m depth as the reference.

from the normal one. In such a case, the deconvolved waveforms would not be simply directly linked anymore to the $P_{11}{}^{SH}(z, 0)$ element of the propagator matrix (Mehta *et al*. 2007a). We must also remember that our data were not rotated in the theoretical transverse direction. Of course, the presence of converted waves (*S*-to-*P*) might also influence the results. Similar mode conversions have been observed in borehole data by Takahashi *et al*. (1992), while Parolai and Richwalski (2004) showed their effect on the horizontal-to-vertical spectral ratio. However, the absence of a clear pulse propagating with *P*-wave velocity before the main pulse propagating with *S*-wave velocity in Fig. 13 seems to work against this hypothesis, although, due to the short traveltime difference between *P*- and *S*-waves over this interval, it might be masked by the dominant *S*-wave pulse. Alternatively, a possible explanation for this observation is that these smaller pulses can be caused by internal *S*-wave reflections (Trampert *et al*. 1993). In such case the high apparent velocity of propagation for the pulse at 50 m depth might be explained by a reflection due to a velocity change occurring between the two sensors at 25 and 50 m depth. Such a velocity change is consistent with the *S*-wave velocity profile in Fig. 3. However, although this mechanism might also explain the velocity of propagation of the pulse between 50 m and 70 m depths (being due to another possible reflection at around 50 m), it would not be able to explain the presence of the small pulse at 25 m depth. Finally, it cannot be excluded that both mechanisms (mode conversion and internal reflection) are acting together.

Figs 14 and 15 show the deconvolution results for the vertical component when the station at the surface or the station at 140 m depth is used as the reference, respectively.

Both figures show an upgoing wave propagating with a velocity consistent with that expected for *P* waves. Fig. 14 also show a main impulse propagating from the top of the borehole to the bottom with a velocity consistent with the *P*-wave velocity.

Note, that no secondary peak that propagates with a velocity consistent with the *S*-wave velocity structure of the site is observed, apart from one in the uppermost 25 m. This, together with the evidence of a secondary peak in the horizontal waveform deconvolution results, might be explained by a stronger *S*-to-*P* conversion than the *P*-to-*S* one or by stronger *S*- than *P*-wave reflections. In fact, while the remarkable changes in the 1-D *S*-wave velocity versus depth estimated by *PS*-logging and array measurements are consistent with significant changes of slopes in the *S*-wave traveltime, for the *P*-wave structure, the variation of velocity seems to be more smooth with depth, except at the boundary between the first and second layer. In fact, the pulse propagation traveltimes are compatible with *P*-wave propagation in a saturated media (therefore with high velocities) already in the second shallow-most layer.

Finally, it is noteworthy that downgoing waves with significant amplitude can be clearly observed down to the deepest accelerometer location. This confirms the hypotesis about the existence and importance of downgoing waves in affecting the spectral ratio that uses as a reference the bottom-most station (Fig. 6).

CONCLUSIONS

A vertical array of accelerometers was installed in Ataköy (western Istanbul) with the aim to improve our understanding of *in situ* soil behaviour and to assess the modelling and parametric uncertainty of employed methodologies for strong-motion site-response analysis, and for shallow geology investigations.

Several geophysical/geotechnical investigations have been carried out at the Ataköy vertical array site. In particular, it was found

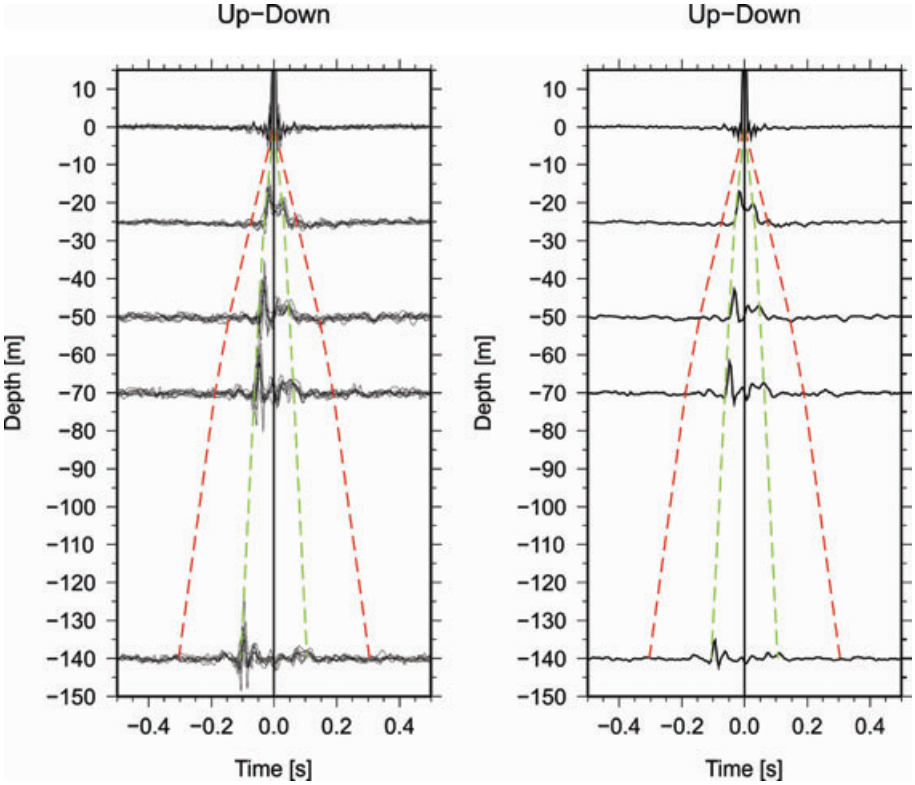

Figure 14. Left-hand panel: the upgoing and downgoing waves obtained by deconvolving vertical component waveforms of each of the sensors with the vertical component waveform recorded by the sensor at the surface. The results for each of the considered earthquakes are shown. Right-hand panel: the stacking of the results depicted in the left-hand panel. The *S*-wave (dashed red line) and the *P*-wave traveltimes (dashed green line) computed from the velocity model derived by using the Parolai *et al*. (2005) inversion scheme are indicated.

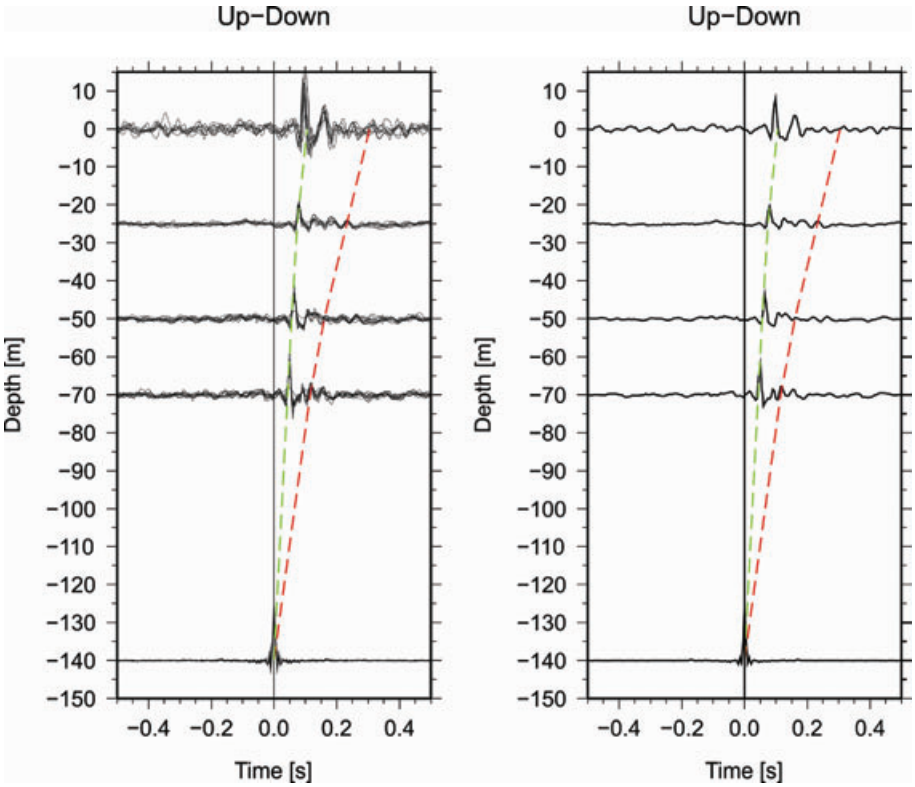

Figure 15. As in Fig. 14, but where the deconvolution was carried out using the station at 140 m depth as the reference.

out that the *S*-wave velocity model derived by the analysis of noise collected by a microarray is in good agreement (in terms of average velocities) with *PS* logging results. The reliability of the *S*-wave velocity profile obtained by microarray analysis was then confirmed by a comparison with the propagation of upgoing and downgoing waves computed by the deconvolution of the recorded wavefield at different depths. Furthermore, due to the joint inversion of dispersion and H/V curves (Parolai *et al*. 2005; Picozzi *et al*. 2005) a velocity profile down to more than 300 m was obtained (although with a larger degree of uncertainty below 230 m depth), showing that the bedrock position is deeper than the deepest accelerometer. These results indicate that micro-arrays are a useful tool in site effect investigation for urban areas. The derived velocity model can also be used to estimate a site response by numerical simulation for comparison with empirical data.

The analysis of the upgoing and downgoing waves obtained by the waveform deconvolution showed, in agreement with previous studies, that they depend on the component of ground acceleration analysed and not on the signal window selected. In particular, pulses propagating with a velocity in agreement with the *S*-wave velocity structure of the site are obtained when considering the horizontal components, while pulses propagating with a velocity compatible with the *P*-wave velocity structure are identified when the vertical component of ground acceleration is used. Since these results were obtained both when a narrow window of signal was selected around the main *P* and *S* arrivals and when the full seismogram was considered, it appears that there is no dominating contribution from surface waves. This might indicate that there are no locally generated high frequency surface waves and that the amplitude of the low frequency surface waves generated by wave propagation in the crust do not vary significantly over the investigated shallow depth range. On the deconvolved horizontal component waveforms, a secondary wavelet propagating with a high apparent velocity, consistent with the *P*-wave velocity structure of the site, was also found. This either suggests *S*-to-*P* mode conversion or/and internal *S*-wave reflections, although effects related to the not-normal incidence of the wavefield cannot be excluded. The data available at hand and the spacing between the sensors does not allow us to draw any definitive conclusion at this moment. A *P*-to-*S* conversion seems to occur in the uppermost 25 m, as shown by the analysis of the vertical components. A larger data set with recordings from earthquakes occurring at positions providing a greater variability in the angle of incidence are necessary to better investigate these issues. In particular, recordings of larger events with higher low-frequency content will help in better separating the transverse from the radial component of ground acceleration, allowing a deeper analysis also in terms of theoretical propagators. However, these evidences suggest that, even when site amplification is mainly related to 1-D effects, the standard practice in engineering seismology of deconvolving the surface recording down to the bedrock using an approximated *S*-wave transfer function (generally valid for vertical incidence of SH waves) might lead to errors in the estimation of the input ground acceleration required in engineering calculations.

Finally, it is worth noting the significant amplitude of downgoing waves down to 70 m and even 140 m depths. This observation provides a warning about the use of shallow borehole recordings as input for numerical simulation of ground motion, and for the derivation of ground motion prediction relationships.

In future studies, the vertical array data set will be exploited for *in situ* measurements of damping, the estimation of soil non-linearity and for assessing *ad hoc* procedures for estimating the input ground motion necessary for engineering calculations.

ACKNOWLEDGMENTS

The vertical array in Ataköy (Istanbul) was realised within the framework of the CEDIM 'Megacity:Istanbul' project. We thank E. Günther for help during the installation of the vertical array. M. Picozzi calculated one of the two *S*-wave velocity profiles by joint inversion of dispersion and H/V curve. We thank O. Özel and the KOERI crew for help during the microarray installation.

One of us (SP) is in debt to D. Bindi for useful discussions and comments on the first draft of the manuscript. The constructive comments of two anonymous reviewers helped to improve the manuscript. R. Milkereit improved figures. K. Fleming kindly improved our English. Figures were generated using GMT (Wessel & Smith 1991).

REFERENCES

Aki, K., 1957. Space and time spectra of stationary stochastic waves, with special reference to microtremors, *Bull. Earthq. Res. Inst.,* **35,** 415–456.

Assimaki, D., Li, W. Steidl, J.H. & Tsuda, K., 2008. Site amplification and attenuation via downhole array seismogram inversion: a comparative study of the 2003 Miyagi-Oki aftershock sequence, *Bull. seism. Soc. Am.,* **98,** 301–330.

Bertero, M. & Boccacci, P., 1998. *Introduction to Inverse Problems in Imaging*. IOP Publishing, Bristol.

Bertero, M., Bindi, D., Bocccaci, P., Cattaneo, M., Eva, C. & Lanza, V., 1997. Application of the projected Landweber method to the estimation of the source time function in seismology, *Inverse Problems,* **13,** 465–486.

Bindi D., Parolai, S., Spallarossa, D. & Cattaneo, M., 2000. Site effects by H/V ratio: comparison of two different procedures, *J. Earthq. Eng.,* **4,** 97–113.

Chiu, H.C. & Huang, H.C., 2003. Estimating the orientation error of the Dahan Downhole Accelerometer using the maximum cross-correlation coefficient between the observed and synthetic waves, *J. Seismol.,* **7,** 493–505.

Chiu, H.C., Huang, H.C., Leu, C.L. & Ni, S.D., 1994. Application of polarization analysis in correcting the orientation error of a downhole seismometer, *Earthq. Eng. Struct. Dyn.,* **23,** 1069–1078.

Dalgic, S., 2004. Factors affecting the greater damage in the Avcilar area of Istanbul during the 17 August 1999 Izmit earthquake, *Bull. Eng. Geol. Environ.,* **63,** 221–232.

Field, E.H., Johnson, P.A., Beresnev, I. A. & Zeng, Y., 1997. Nonlinear ground-motion amplification by sediments during the 1994 Northridge earthquake, *Nature,* **390,** 599–602.

Halliday, D. & Curtis, A., 2008. Seismic interferometry, surface waves and sources distribution, *Geophys. J. Int.,* **175**(3), 1067–1087.

Horike, M., 1985. Inversion of phase velocity of long period microtremors to the S-wave velocity structure down to the basement in urbanized areas, *J. Phys. Earth,* **33,** 59–96.

Hough, S.E., Seeber, L., Rovelli, A., Malagnini, L., De Cesare, A., Selvaggi, G. & Lerner-Lam, A., 1992. Ambient noise and weak motion excitation of sediment resonances: results from the Tiber Valley, Italy, *Bull. seism. Soc. Am.,* **82,** 1186–1205.

Huang, H.C., Huang, S.W. & Chiu, H.C., 2005. Observed evolution of linear and nonlinear effects at the Dahan Downhole Array, Taiwan: analysis of the September 21, 1999 M 7.3 Chi Chi Earthquake sequence, *Pure appl. Geophys.,* **162,** 1–20.

Lobkins, O.I. & Weaver, R.L., 2001. On the emergence of the Green's function in the correlation of a diffuse field, *J. acoust. Soc. Am.,* **110,** 3011–3017.

Konno, K. & Ohmachi, T., 1998. Ground-motion characteristic estimated from spectral ratio between horizontal and vertical components of microtremor, *Bull. seism. Soc. Am.,* **88,** 228–241.

Mehta, K., Snieder, R. & Grazier, V., 2007a. Extraction of near-surface properties for a lossy layered medium using the propagator matrix, *Geophys. J. Int.,* **169,** 2171–280.

Mehta, K., Snieder, R. & Grazier, V., 2007b. Downhole receiver function: a case study, *Bull. seism. Soc. Am.,* **97,** 1396–1403.

Nakamura, Y., 1989. A method for dynamic characteristics estimations of subsurface using microtremors on the ground surface, *Q. Rept. RTRI Jpn.,* **30,** 25–33.

Nigor, R.L. & Imai, T., 1994. The suspension P-S velocity logging method, in *Proceedings of the XIII International Conference on Soil Mechanics and Foundation Engineering*, 5–10, January 1994, New Delhi, India.

Ohori, M., Nobata, A. & Wakamatsu, K., 2002. A comparison of ESAC and FK methods of estimating phase velocity using arbitrarily shaped microtremor analysis, *Bull. seism. Soc. Am.,* **92,** 2323–2332.

Okada, H., 2003. *The Microtremor Survey Method, Geophysical Monograph Series,* Vol. 12, American Geophysical Union, Washington

Parolai, S. & Richwalski, S.M., 2004. The importance of converted waves in comparing H/V and RMS site response, *Bull. seism. Soc. Am.,* **94,** 304–313.

Parolai, S., Picozzi, M., Richwalski, S.M. & Milkereit, C., 2005. Joint inversion of phase velocity dispersion and H/V ratio curves from seismic noise recordings using a genetic algorithm, considering higher modes, *Geophys. Res. Lett.,* **32,** L01303, doi:10.1029/2004GL021115.

Parolai, S, Richwalski, S.M., Milkereit, C. & Faëh, D., 2006. S-wave velocity profiles for earthquake engineering purposes for the Cologne area (Germany), *Bull. Earthq. Eng.,* **4,** 65–94.

Picozzi, M. & Albarello, D., 2007. Combining genetic and linearized algorithms for a two-step joint inversion of Rayleigh wave dispersion and H/V spectral ratio curves, *Geophys. J. Int.,* **169,** 189–200.

Picozzi, M., Parolai, S. & Richwalski, S., 2005. Joint inversion H/V ratios and dispersion curves from seismic noise: estimating the S-wave velocity of bedrock, *Geophys. Res. Lett.,* **32(**11), L11308, doi:10.1029/2005GL022878.

Picozzi, M., Strollo, A., Parolai, S., Durukal, E., Özel, O., Karabulut, S., Zschau, J. & Erdik, M., 2009. Site characterization by seismic noise in Istanbul, Turkey, *Soil. Dyn. Earthq. Eng.,* **29**(3), 469–482.

Safak, E., 1997. Models and methods to characterize site amplification from a pair of records, *Earthq. Spectra, EERI*, **13,** 97–129.

Scherbaum, F., Hinzen, K.-G. & Ohrnberger, M., 2003. Determination of shallow shear wave velocity profiles in Cologne, Germany area using ambient vibrations, *Geophys. J. Int.,* **152,** 597–612.

Schuster, G.T., Yu, J., Sheng, J. & Rickett, J., 2004. Interferometric/daylight seismic imaging, *Geophys. J. Int.,* **157,** 838–852.

Seale, S. & Archuleta, R., 1989. Site amplification and attenuation of strong ground motion, *Bull. seism. Soc. Am.,* **79,** 1673–1696.

Shapiro, N.M. & Campillo, M., 2004. Emergence of broadband Rayleigh waves from correlations of ambientseismic noise, *Geophys. Res. Lett.,* **31,** L07614, doi:10.1029/2004GL019491.

Snieder, R., Sheiman, J. & Calvert, R., 2006. Equivalence of the virtual-source method and wave-field deconvolution in seismic interferometry, *Phys. Rev. E,* **73,** 066620.

Takahashi, K., Ohno, S., Takemura, M., Ohta, T., Sugawara, Y., Hatori, T. & Omote, S., 1992. Observation of earthquake strong motion with deep borehole: generation of vertical motion propagating in surface layers after S-arrival, in *Proceedings of the 10th World Conference on Earthquake Engineering,* Madrid, Spain, Vol. 3, pp. 1245–1250. Balkema, Rotterdam.

Tibi, R. *et al*., 2001. Rupture processes of the 1999 August 17 Izmit and November 12 Düzce (Turkey) earthquakes, *Geophys. J. Int.,* **144,** F1–F7.

Tikhonov, A.N. & Arsenin, V.Y., 1977. *Solution of Ill-Posed Problems,* Wiston/Wiley, Washington.

Trampert, J., Cara, M. & Frogneux, M., 1993. SH propagator matrix and Qs estimates from borehole- and surface-recorded earthquake data, *Geophys. J. Int.*, **112,** 290–299.

van Vossen, R., Trampert, J. & Curtis, A., 2004. Propagator and wave-equation inversion for near-receiver material properties, *Geophys. J. Int.,* **157,** 796–812.

van Vossen, R., Curtis, A. & Trampert, J., 2005. Subsonic near-surface P-velocity and low S-velocity observation using propagator inversion, *Geophysics,* **70,** R15–R23.

Wessel, P. & Smith, W.H.F., 1991. Free software helps map and display data, *EOS Trans. AGU,* **72,** 441, 445–446.

Xia, J., Miller, R.D., Park, C.B. & Tian G., 2003. Inversion of high frequency surface waves with fundamental and higher modes, *J. appl. Geophys.,* **52,** 45–57.

Yamanaka, H. & Ishida, H., 1996. Application of Generic algorithms to an inversion of surface-wave dispersion data, *Bull. seism. Soc. Am.,* **86,** 436–444.

ZETAŞ®, 2006. Factual report on drilling for strong ground motion network, 03/04/2006. ZETAŞ® Zemin Teknolojisi A.Ş.